First-principles study of charge-density waves on Cu surfaces covered by In, Pb, and Bi atoms: Analysis of electronic structure and surface phonons

Tatsuhiko Ohto,* Akihiro Nojima, and Koichi Yamashita
Department of Chemical System Engineering, Graduate School of Engineering, The University of Tokyo, Tokyo 113-8656, Japan

Hisao Nakamura†
Nanosystem Research Institute (NRI) RICS, Advanced Industrial Science and Technology (AIST), Central 2, Umezono 1-1-1, Tsukuba, Ibaraki 305-8568, Japan

(Received 17 November 2009; revised manuscript received 21 May 2010; published 8 October 2010)

We performed a first-principles density-functional calculation to investigate the difference in the mechanisms of phase transitions for In/Cu(001) and W(001). We also explain the origins of surface states of In, Pb, and Bi/Cu(001)-0.5 ML having $c(2\times2)$ structure that cause a phase transition via the generation of a charge-density wave (CDW). The perfect theoretical/experimental agreement for the wave numbers of nesting vectors corresponding to the well-nested surface states of In and Pb/Cu(001)-0.5 ML is reported. Band-structure analysis suggests a common mechanism of CDW transition for In and Pb/Cu(001)-0.5 ML. The absorption of In and Pb on Cu(001) leads to a reduction in the energy of the band composing the edge of bulk band gap. As a result, the band enters the bulk band gap and has the character of the surface state. Since these surface states compose a well-nested Fermi surface, CDW transition would be induced. In addition, we studied the relationship between the lattice distortions and the band dispersions of the surface states of In/Cu(001)-0.5 ML and W(001) in terms of the Jahn-Teller effect (JTE). While we find promoting modes that resolve the degeneracy of surface states of W(001), any surface-localized mode of In/Cu(001) does not split the band of surface state. Therefore, the static electron-phonon interaction of In/Cu(001) is weak. We propose that the dynamic JTE contributes to the CDW transition of In/Cu(001) and the dynamic nature is related to the spatial coherence length of the CDW.

DOI: 10.1103/PhysRevB.82.155415 PACS number(s): 71.15.Mb, 71.18.+y, 71.45.Lr

I. INTRODUCTION

Phase transitions in reduced dimensions have been investigated in decades. The metal-insulator transition caused by the electron-phonon coupling with the overlap of the Fermi surface at low temperature, is referred to as the Peierls transition. A charge-density wave (CDW), which is a standing wave of charge density having the same periodicity as that of the lattice distortion, follows the Peierls transition.[1,2] Nanometric electronic device technology would extremely take advantage of a deeper knowledge of the Peierls transition since it is associated with changes in transport properties in low-dimensional structures such as interfaces. Phase transitions due to CDWs have been observed for several bulk conductors and/or metal surfaces covered with adsorbed atoms.[3,4]

A CDW at surface is generally categorized as a strong-coupling CDW (see below). Because of the strong electron-phonon coupling, its **k** dependence often masks the instability induced by the overlap of the Fermi surface (nesting).[5–8] Moreover, the order-disorder transition usually associates with the strong-coupling CDW.[9–11] These effects make it difficult to predict the transition temperature or the periodicity of the CDW state. Therefore, classification of the surface CDW using specific indicators has been discussed eagerly.[12–14]

The mechanism of the associated order-disorder phase transition can be classified by the strength of electron-phonon coupling, which can be determined from the energy gap of the CDW state, through theoretical treatment of the Peierls transition. In the weak-coupling case, mean-field theory can be applied. In such a case, the energy gap emerges continuously at the transition temperature with a concomitant periodic lattice distortion. On the other hand, when the energy gap is larger than (typically) 100 meV, the transition is categorized as a strong-coupling case, for which mean-field theory breaks down. In addition, the length of coherence for the CDW state is a useful parameter for characterizing the transition mechanism. The length of coherence is often represented by the CDW correlation length, which is the size of a CDW wave packet and calculated by summing the electron wave functions along k space where the band gap forms. Usually, the length of coherence in the CDW state for weak coupling is greater than that for strong coupling.

A typical case of a strong-coupling CDW at a metal surface is the reconstruction from $p(1\times1)$ to $c(2\times2)$ on W(001).[12–15] See Fig. 1 for the real-space structures of W(001) and their Brillouin zones. In the ground state, a new periodic potential due to a frozen phonon modifies electron structures and produces an energy gap on the Fermi surface of the high-temperature phase of a metal. W(001) has a phonon instability at M point on a high-symmetry $p(1\times1)$ phase and the vector $\overrightarrow{\Gamma\bar{M}}$ coincides with the nesting vector of the Fermi surface. Softening of the $\bar{M}_5$ phonon mode is observed by inelastic He scattering upon approaching the transition temperature.[16,17] In addition, electronic state calculations show that a band gap appears at the position of the Fermi surface and that the CDW ground state is more stable than the high-temperature phase.[15,18] This is an evidence of CDW transition on W(001) from a $p(1\times1)$ to $c(2\times2)$ structure.

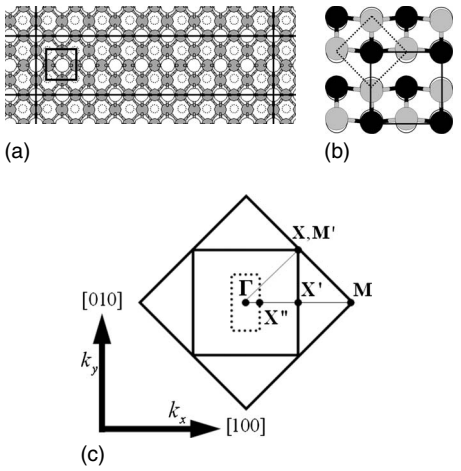

FIG. 1. (a) Top view of the metal/Cu(001)-0.5 ML surface (metal=In, Pb, or Bi). Only first Cu layer is shown for the clarity. The c(2×2) unit cell is shown by the small square. The large square means $(9\sqrt{2}\times 2\sqrt{2})R45°$ unit cell Dotted circles means the position of second layer of In for In/Cu(001)-1.0 ML structure. (b) Top view of W(001) surface. Atoms in the first and second layers are denoted by shaded and solid circles. Open circles show the highly symmetric positions of atoms. The solid square and the dotted diamond show the unit cell of c(2×2) and p(1×1), respectively. (c) Brillouin zones and highly symmetric points of p(1×1) and c(2×2) periodicity of the Cu(001) surface. Those of W(001) are the same. The small dotted rectangular means the Brillouin zone of $(9\sqrt{2}\times 2\sqrt{2})R45°$ unit cell.

The larger band gap (~2 eV) than that can be predicted from the transition temperature with mean-field theory and the order-disorder behaviors of lattice[19] are sufficient to classify this transition as a strong-coupling one.

Recently, Aruga[13,14] observed a CDW transition for In/Cu(001) and its mechanism differs from, for example, that of W(001). In/Cu(001) has two phase transitions that are reversible with temperature at coverages of 0.5 and 0.63 ML.[20,21] According to Refs. 20 and 21, both systems have well-nested Fermi surfaces at high temperature but they partly disappear and band-gap openings are observed at low temperature. These features indicate CDW transitions. Above Fermi surfaces are produced by surface resonance states with Cu 4*sp* and In 5*sp* orbitals, and these states become stable with increasing coverage of In atoms. The mechanism of the phase transition of In/Cu(001)-0.63 ML is being actively investigated because the whole band gap of the low-temperature phase can be observed by angle-resolved photoemission spectroscopy.[13,22–24] Hatta *et al.*[22,23] examined the behaviors of band gaps and lattice distortion separately and found that the temperature dependence of the band gap could be described by mean-field theory, i.e., the weak-coupling CDW, while the order-disorder behavior of lattice was observed as the strong-coupling CDW. They suggested that the length of coherence played a role in the critical deference of the transition between In/Cu(001) and W(001).

The CDW transitions of several metal atom/Cu(001)-0.5 ML surfaces, e.g., Pb[c(2×2)−c$(5\sqrt{2}\times\sqrt{2})R45°$] (Ref. 25) and Sn[c(2×2)−c$(3\sqrt{2}\times\sqrt{2})R45°$],[26] have been observed. These phase transitions are reversible with the temperature. A well-nested Fermi surface is observed at the high temperature while a band gap opens in the low-temperature regime for both cases. These features are quite similar with that of In/Cu(001). The observed surface states, which should be responsible for surface structure transition, have distributions similar to those of the bulk band-gap edge. Blanco *et al.*[26] suggested that the Cu(001) substrate has a role in the instability and that adatoms are the trigger of the distortion. On the other hand, Aruga[13] proposed that these heavier *p*-block metals interact with the substrate with only the valence *p* orbital having energy close to the Cu *sp* bands because the core electrons have very low energy. While the knowledge of mechanisms of those transitions will help us to better rationalize the categorization of surface CDWs, the details of the modulation of the lattice are not clear from an atomistic view. There are three questions to be answered. (1) Is the CDW ground state of In (and other atoms) on Cu(001) really more stable than the high-symmetry state energetically? (2) Which phonon modes are promoting modes for the phase transition? (3) Which band (or surface) state dominates the electron-phonon couplings and modulation, i.e., are the CDW transitions of In (and other atoms) on Cu(001) triggered by Cu(001) surface and are their mechanisms different from that of W(001)? Hence, it is important to determine and compare the electronic states of these systems to understand better the CDW and analysis of the electronic structure on the basis of first-principles calculations is highly desired.

Recently, Gao *et al.*[27] calculated the electronic structure of the In/Cu(001)-c(2×2). They proposed a nesting wave number of 0.38 $Å^{-1}$, which is slightly larger than the experimental value, i.e., 0.31 $Å^{-1}$.[20,27] They also concluded that the bonding p_x and p_y bands relating to In adatoms compose a well-nested Fermi surface with coverage of 1.0 ML while it was found that the correct coverage rate was 0.5 ML for the c(2×2) structure.[21] However, the experimental results show that the formation of a well-nested Fermi surface is caused by the mixed electronic states of Cu and In adatoms: thus the prediction by Gao *et al.* conflicts with the experimental observation. In addition, as far as we know, there is no detailed first-principles calculation for Cu surfaces covered by other metal adatoms.

In the present study, we focus on the origins of surface states, their relationship to surface phonon modes, and the mechanism of the lattice modulation in the context of the classification of CDWs. We first make systematic calculations for Cu(001) covered by In, Pb, and Bi metal adatoms, where all systems have highly symmetric c(2×2) phases. The origins of the experimentally detected surface states are determined as well as their Fermi-nesting vectors. The role of Cu(001) surface is also discussed. Next, to identify the concerns between energy stabilization and lattice modulation by the promoting mode directly, we adopt the scheme of the Jahn-Teller effect (JTE). This approach uses phonon mode displacement as the order parameter (i.e., "real-space description" for the Peierls transition) and also the formation of the band gap as an indicator of the transition. The higher-to-lower symmetric structure distortion and the strong electron-phonon interactions, referred to as vibronic coupling, can be often described as the result of the static JTE. Thus, we analyze the relaxation of the structure of W(001) to show the

validity of the JTE scheme. We then perform the same analysis for In/Cu(001) and determine the difference in the mechanism between the standard strong-coupling CDW and that for In/Cu(001).

The organization of this paper is as follows. In Sec. II, we briefly review the CDW and then describe our computational scheme for applying first-principles calculations. In Sec. III, we show the resulting electronic structures for each system and analyze the surface state and Fermi surfaces with nesting. We investigate the surface phonon and vibronic interactions in Sec. IV. In addition, we discuss the type of CDW and strength of vibronic coupling. Conclusions are presented in Sec. V.

II. THEORETICAL BACKGROUND AND COMPUTATIONAL METHOD

A. Brief survey of CDWs

A CDW state is a ground state that results from the Peierls transition driven by electron-phonon interaction in metallic materials. Peierls instability can be characterized by the anomaly of a component of the dynamical matrix D_2, which is the second-order perturbation correction of the band energy caused by electron-phonon interaction,

$$D_2^{\alpha\beta}(\kappa,\kappa';q) = -\sum_{\substack{\kappa\mu\mu' \\ k'=k+q}} \frac{f_{k'\mu'} - f_{k\mu}}{\varepsilon_{k\mu} - \varepsilon_{k'\mu'}} g^{\kappa\alpha}_{k\mu,k'\mu'} g^{\kappa'\beta}_{k'\mu',k\mu}, \quad (1)$$

where $\varepsilon_{k\mu}$ is the band energy and the indices k and μ represent the wave vector and band label, respectively. The term $f_{k\mu}$ is the Fermi occupation number and $g^{\kappa\alpha}$ is the electron-ion coupling constant, where κ and α are the ion index and label of the Cartesian coordinates, respectively. From Eq. (1), we find that the term D_2 includes the electron susceptibility function χ_0. The susceptibility χ_0 has a singularity when Fermi surfaces overlap, which is often referred to as nesting. For simplicity of explanation, we take a one-dimensional electron gas system, although the fundamental mechanism is the same as that for two-dimensional systems. In the one-dimensional system, χ_0 diverges at $T=0$ and $q=2k_F$. As a result, the phonons soften and freeze with decreasing temperature when the phonon wave vector q is equal to $2k_F$. Owing to the frozen phonon, the periodicity of the system is modified, and an energy band gap forms at $q=2k_F$ for a low-symmetry phase and the total energy decreases. This ground state is referred to as the CDW state because the periodicity of the lattice ($=2k_F$) is the same as that of a standing wave of the charge density responding to the potential of the lattice via χ_0. Hence, *in general*, the overlapping of Fermi surfaces is required for the formation of the CDW.

When we focus on the strength of electron-phonon interaction, the CDW transitions are usually classified as weak-coupling and strong-coupling ones. The electron-phonon coupling strength is usually determined from the resulting magnitude of the band gap. However, further classification is possible for observed CDW transitions of metal surfaces (i.e., as either a strong-coupling and short-coherence CDW or as a strong-coupling and long-coherence CDW) using the spatial coherence length of the CDW as the other measurement. The spatial coherence length, or the CDW correlation length, is determined from the region δk in k space, where the band gap forms. Obviously, this depends on the bandwidth of the surface state. The correlation length of the CDW is defined as

$$\xi_{\mathrm{CDW}} = \frac{2\pi}{\delta k} \quad (2)$$

and it is estimated as $\xi_{\mathrm{CDW}} \approx 60$ Å for In/Cu(001) and $\xi_{\mathrm{CDW}} \approx 7$ Å for W(001).[13] The transition temperatures of electrons and lattices dramatically differ according to ξ_{CDW}. In the case of a low value of ξ_{CDW}, an order-disorder transition process takes place at a temperature much lower than that expected from mean-field theory. The CDW in W(001) is a typical strong-coupling and short-coherence system. On the other hand, the band gap disappears at a temperature a little above that for the order-disorder process, regardless of the large band gap in the case of a high value of ξ_{CDW}.

As briefly stated in Sec. I, the **k**-dependent $g^{\kappa\alpha}$ in Eq. (1) often masks χ_0 in the case of a strong-coupling CDW as usually observed on metal surfaces, i.e., the periodicity of the CDW is modified from that is predicted from a well-nested Fermi surface.[5–8] While the Fermi surface is expected to be involved in the transition of In/Cu(001),[24] we should evaluate the electron-phonon coupling to understand the modulation of lattice more precisely. To analyze the transition mechanism and classifications of the CDW from an atomistic view further, it is useful to consider the phonon dispersion and then the change in the surface state during the transition as well as determine the nesting vector. In the present study, we mainly focus on the Cu(001) surface covered by In, Pb, and Bi atoms and conduct an analysis based on first-principles calculations. In the following sections, we describe the first-principles calculation scheme for the Cu(001) surface covered by In, Pb, and Bi atoms.

B. Computational procedure

In order to investigate the origins of the surface states, first we considered In, Pb, and Bi/Cu(001)-0.5 ML, all of which have symmetric c(2×2) structures[21,28,29] for the monolayer to investigate the origins of the surface states. The chemical characteristics of adatoms differ slightly and their low-temperature phases are $(9\sqrt{2}\times 2\sqrt{2})R45°$,[21] $c(5\sqrt{2}\times\sqrt{2})R45°$,[25] and $c(9\sqrt{2}\times\sqrt{2})R45°$ (Ref. 29) for In, Pb, and Bi, respectively. Nevertheless, their phase transitions [from c(2×2) to the structure derived from c(2×2)] are considered to have a mechanism similar to that for In/Cu(001).[12]

We also examined the c(2×2) phase of In/Cu(001)-1.0 ML so that we can discuss the results reported in Ref. 27 that show that coverage of 1.0 ML is required for the formation of a well-nested Fermi surface. While the observed structure is $(\sqrt{20}\times\sqrt{20})R63.4°$ at room temperature,[21] we assumed that In atoms form a bilayer structure with both layers having 0.5 ML coverage of In atoms with a c(2×2) arrangement as described in Ref. 27. All In atoms occupy hollow sites of underlying layers, as shown in Fig. 1(a).

The coexistence of the features triggered by the weak- and strong-coupling CDW was proposed for a In/Cu(001)-

0.63 ML, whose structure transits from $p(2\times2)$ to $c(4\times4)$. However, it is somewhat inconvenient to analyze and calculate this 0.63 ML system directly because atomistic details in the high-temperature phase are not clear.[13,22–24] In the present study, we assumed that the phase transition mechanisms for 0.5 and 0.63 ML coverages are of the same type, i.e., strong-coupling and long-coherence CDWs. This assumption is valid because the band gap of the 0.5 ML system is greater than 400 meV, which is sufficiently large to categorize the system as having strong coupling. Moreover, the Fermi surfaces of both systems have the same origin and the correlation lengths of the systems are almost the same.[5,13]

All calculations of the $c(2\times2)$ structures were based on density-functional theory (DFT) (Refs. 30 and 31) and used Vienna *ab initio* simulation package (VASP) software.[32] The wave functions were expanded in a plane-wave basis set and the effective potential of the ions was described using projected augmented waves.[33,34] The plane-wave energy cutoff was 510 eV. The nonspin-polarized version of the generalized gradient approximation [PW-91 GGA (Ref. 35)] was employed for the exchange-correlation functional.

The adsorbate-substrate system was modeled as a slab with seven layers of fcc-(100)-stacked copper atoms and 25 Å vacuum. Each layer had two Cu atoms and the supercell had adsorbates on both sides. The Brillouin zone of the $c(2\times2)$ cell was sampled in a $6\times6\times1$ Monkhorst-Pack grid.[36] The atomic positions were optimized using a quasi-Newtonian algorithm and relaxed until the average force on each atom was less than 10^{-2} eV/Å. The optimized structure and charge density were used to calculate the band structure and partial charge densities. The band structure of the system was determined by calculating the Kohn-Sham eigenvalues along the irreducible wedge $\Gamma-X'-M'-\Gamma$ of the surface Brillouin zone at 100 k points.

We calculated the bulk fcc structure of Cu to check the validity of the conditions. When the unit cell was taken as that of the Bravais lattice, the equilibrium lattice constant of fcc Cu determined using PW-91 GGA was 3.635 Å, which is in reasonable agreement with the measured value of 3.61 Å.[37] In addition, we reproduced the same calculation results[38,39] for both the bulk band structure and Cu(001) surface band structure.

Next, we considered the electron-phonon coupling of the $c(2\times2)$ and $(9\sqrt{2}\times2\sqrt{2})R45°$ structures of the In/Cu(001)-0.5 ML. We did not calculate low-temperature phases for Pb and Bi because of the change in the coverage during phase transitions. To calculate the phonon dispersions, we adopted the SIESTA software package,[40] which is based on DFT,[30,31] with slight modification. We used the Perdew-Burke-Ernzerhof[41] functional and a single-ζ polarized basis set. In addition, we used the Troullier-Martins norm-conserving pseudopotential[42] with the Kleinman-Bylander nonlocal projector.[43] The number of layers was reduced to three and In atoms were adsorbed on only one side of the slab. The Brillouin zones of the $c(2\times2)$ and $(9\sqrt{2}\times2\sqrt{2})R45°$ cells were sampled in $6\times6\times1$ and $2\times6\times1$ k grids, respectively. To check the validity of the calculation, we compared the Fermi vectors of the surface state (and band structure) obtained by SIESTA with the results obtained by VASP, as stated above. Although the number of layers in the slab, the adopted functional, and the basis set all differed, the results obtained by VASP and SIESTA agreed well for our purpose. When we optimized the $(9\sqrt{2}\times2\sqrt{2})R45°$ structure, we did not observe surface reconstruction; i.e., In atoms remained in the fourfold hollow sites of the Cu substrate, as shown in Fig. 1.

In the phonon calculations, we employed the standard frozen-phonon approximation as follows. In the case of the $c(2\times2)$ structure, we took nine unit cells as the supercell in real space and then relaxed only the atoms in the central unit cell to estimate the dynamical matrix. Since the unit cell of the $(9\sqrt{2}\times2\sqrt{2})R45°$ structure was sufficiently large, we estimated the rigorous Hessian only for the unit cell and then approximated the dynamical matrix as a block-diagonal matrix including the phase factor correction by introducing a truncation of the interactions between atoms in the central unit cell and atoms in other cells. In addition, all In and Cu atoms of the layer beneath the In monolayer were displaced. The above frozen-phonon approach was sufficient for our purpose of determining the surface modes because most of the surface state of In/Cu(001)-0.5 ML should be localized.

III. ELECTRONIC STRUCTURES

A. In/Cu(001)-0.5 ML and In/Cu(001)-1.0 ML

We first calculated the adsorption structures of In/Cu(001)-0.5 ML with a $c(2\times2)$ phase.[21,28,29] The calculation results show that absorption at the hollow site is energetically most stable. This agrees with previous theoretical results for the adsorption of In atoms on a Cu(001) surface.[44] Table I gives the vertical positions of adatoms measured for the Cu(001) surface and it is seen that our calculation reproduces the structures determined in previous theoretical and experimental studies.

Figure 2 shows the calculated band structure of the In/Cu(001)-0.5 ML surface plotted along the high-symmetry directions of the $c(2\times2)$ surface Brillouin zone, which is half the area and 45° rotated with respect to the Brillouin zone of clean Cu(001). The energy bands of the In layer standing freely are also shown. The bonding bands (BBs) induced by In atoms, which have p character and large charge-density amplitude around the In layer, are marked as dotted lines in Fig. 2. The bands slightly apart from the projected bulk band of clean Cu(001) are labeled S1. The other bands, labeled S2, relate to the surface states.

In Fig. 2, it is shown that S1 is slightly shifted downward from the projected bulk band region and has a distribution similar to that of the experimental result still in Fig. 2 along the $\Gamma-X'$ line. The energies of S1 differ by about 1 eV compared with values obtained by the photoemission spectroscopy (PES),[21] but the shape of the distribution is nearly the same as that obtained by PES along the $\Gamma-M'$ line. Since experimentally observed bands relating to the surface state lie in the bulk band gap, it is possible that S1 is generated by the adsorption of In atoms and has the character of the surface state. Hence, we checked the difference in the charge-density distribution between S1 and the bulk band edge of the clean Cu (001) surface, which is labeled B.

TABLE I. Adsorption positions of monolayer and bilayer In/Cu(001), Pb/Cu(001), and Bi/Cu(001) systems for hollow-site adsorption structures. H is the vertical height of the adatom above the Cu(001) plane. In addition, calculated nesting vectors and comparisons with previous works are shown.

	H (Å)	Ref.	k_F (Å^{-1})	Ref. Expt.	Ref. Calc.
In/Cu(001)-0.5 ML	2.12	2.19 (Ref. 27)	0.31 (S1) 0.6 (BB)	0.30 (Ref. 20)	
In/Cu(001)-1.0 ML (bilayer structure)[a]	2.08	2.11 (Ref. 27)	0.40 (BB)		0.38 (unrelaxed) (Ref. 27)
	2.11	2.11 (Ref. 27)			0.41 (relaxed) (Ref. 27)
Pb/Cu(001)-0.5 ML	2.21	2.29 (Ref. 45)	0.29	0.29 (Ref. 25)	
Bi/Cu(001)-0.5 ML	2.13	2.27 (Ref. 46)	0.27		

[a]The upper section shows the vertical height of the intermediate In layer from the substrate and the lower section shows that of the outermost In layer from the In layer beneath.

Figure 3 shows the charge-density distributions of S1 and B at Γ point and the crossing point with the Fermi energy. Both Figs. 3(a) and 3(b) show large charge-density amplitude around the center of the slab, and thus S1 and B have almost the same electronic character over a wide region. However, S1 and B have completely different characters in the region close to the crossing point of the bands and Fermi energy. As shown in Figs. 3(d) and 3(e), while B has large charge-density amplitude around the center of the bulk, most of the charge density of S1 is concentrated on the interface of the outermost Cu and adatom. Therefore, the energy of the bulk band B decreases owing to the change in potential induced by adsorption. B is then pushed into the bulk band gap, and it has the character of a surface state; thus, B changes to S1. To confirm that S1 corresponds to the experimentally observed band, we calculated the Fermi surface of S1.

The calculated Fermi surface of the surface resonance band S1 for the In/Cu(001)-0.5 ML-c(2×2) structure is shown in Fig. 4. S1 has a Fermi surface along the bulk band edge of Cu(001), which is represented by a shaded area. S1 shifts downward into the projected bulk band gap while the difference between S1 and B is less than 0.01 Å^{-1}. The Fermi wave number of the quasisquare-shaped Fermi surface, which has a distribution similar to that of the bulk band, is 0.31 Å^{-1} (from Γ point along the k_x axis as shown in Fig. 4) and this value agrees well with the experimental value of 0.30 Å^{-1}.[20] This result for the Fermi wave vector and surface suggests nesting of $Q_1 = 2k_F/3$. This non-$2k_F$ nesting of Q_1 is come from the **k**-dependent electron-phonon coupling.[5,8,12] Figure 4 also shows the Fermi surface of the bands of the freestanding In layer and the BB. The fact that the energies and distributions of the two bands being quite

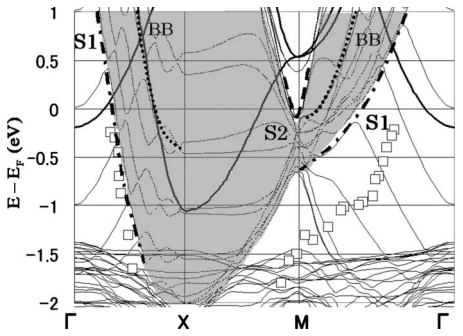

FIG. 2. Band structure of In/Cu(001)-0.5 ML. The shaded area shows the clean Cu(001) projected bulk band. The broad solid lines show the band structure of the freestanding In layer. The dotted-dashed and dashed lines are surface resonance states S1 and S2, respectively. The dotted lines show In atom-induced states labeled as the BB. The surface-state bands measured by PES (Ref. 20) are shown by small squares.

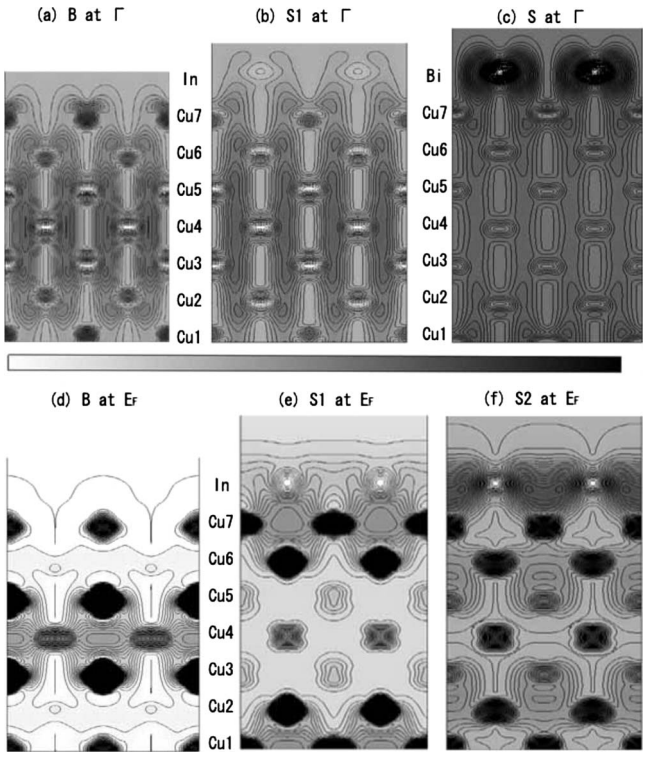

FIG. 3. Comparison of the edge of the bulk band of clean Cu(001) with the surface resonance state of In/Cu(001) or Bi/Cu(001). The pictures show the charge-density distribution written by VESTA (Ref. 47). B is the edge of the projected bulk band of clean Cu(001), and S1 and S are the surface resonance states of In/Cu(001) and Bi/Cu(001), respectively. S2 is a localized surface state of In/Cu(001). A darker area indicates higher charge density.

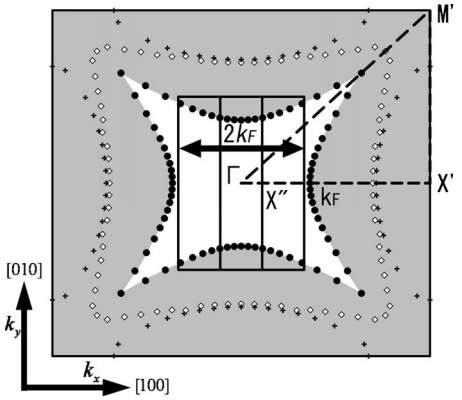

FIG. 4. Fermi surface of the surface states on the In/Cu(001)-0.5 ML-c(2×2) structure. The large square and small rectangles show the surface Brillouin-zone boundaries of the c(2×2) and $(9\sqrt{2}\times 2\sqrt{2})R45°$ structures, respectively. The shaded area represents the projected bulk band of clean Cu(001). The filled circles, open diamonds, and crosses show the crossing points of S1, BB, and the bands of the freestanding In layer with the Fermi energy. The dashed line is the symmetry line shown in Fig. 1. X″, or 1/9Γ-X′, is the edge of the $(9\sqrt{2}\times 2\sqrt{2})R45°$ Brillouin zone along the k_x axis. $2k_F$ is the distance between most flat parts of the Fermi surface of S1. The k_F vector is from Γ point to the crossing point of the S1 edge and k_x axis.

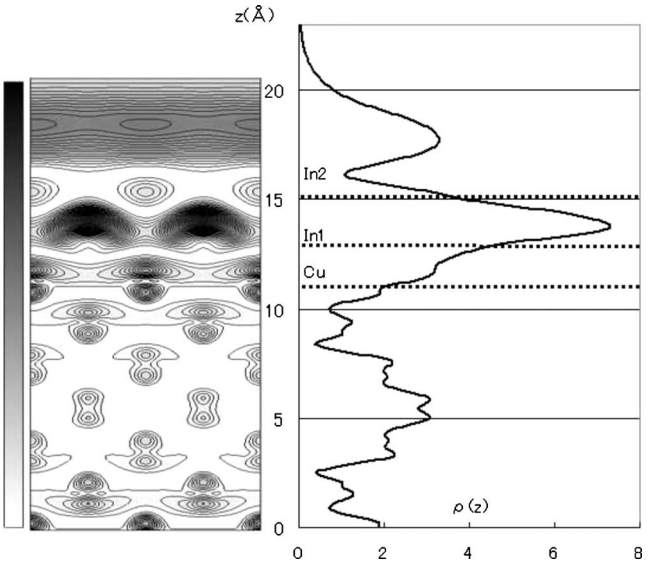

FIG. 5. Two-dimensional charge distribution of the In-induced state of In/Cu(001)-1.0 ML and the average charge density in the z direction of the slab.

similar leads to the origin of the energy of the BB; i.e., the energy of the BB is determined only by the arrangement of In. However, the BB has a character completely different to that of the experimentally observed band because it exists within the bulk band continuum and the wave number of its nesting vector is 0.60 $Å^{-1}$. In addition, our calculation shows that the BB has large charge-density amplitude around the In atoms at Γ point, although the amplitude reduces near E_F.

From the comparison of the band structure with that reported in Ref. 27, we see that the reported In-induced state relates to the BB because they have a similar distribution and the same characteristic of the In p orbital. The BB lowers its energy and composes a Fermi surface in In/Cu(001)-1.0 ML but does not produce a CDW. Hence, we conclude that we have found the occurrence of a decrease in the energy of the bulk band. Furthermore, our first-principles calculation reproduces the value of the Fermi wave vector.

Our results are supported by other studies of the charge-density distribution. Recently, Aruga *et al.* predicted that the origin of the observed surface resonance state is the 4*sp* orbital of Cu and 5*sp* orbital of In, and they calculated wave functions of two surface states around M′ point using a 25-layer In/Cu(001)-0.5 ML slab model.[13] They noted that the surface state that causes the Fermi-surface nesting penetrates to a depth of at least 10–20 layers, and another surface state lying above the bulk band continuum at point M shows strong localization at the surface. In our calculation, we found two surface states, labeled S1 and S2 in Figs. 3(d) and 3(e) along Γ−M′. Although the thickness of our slab model is insufficient for analyzing the penetration length of the charge densities into the bulk, our calculated charge distributions agree reasonably with those presented in Ref. 13. The most important point is that the region of high charge density for S1 shifts from the bulk to the surface, becoming closer to the Fermi energy. These results show that S1 has the *sp*-orbital characteristics of both bulk Cu and the In atom and causes the Peierls transition.

Next, we calculated the 1.0 ML coverage, which has bilayer submonolayer structure, to examine our prediction that the BB gains energy in the case of 1.0 ML coverage as well as to determine the nested Fermi surface and compare with the result presented in Ref. 27. The resulting total energy shows that this structure is the most stable formulation. From the band dispersion, we found that the p-character band of In composes the well-nested Fermi surface. The calculated wave number was 0.40 $Å^{-1}$, which is in good agreement with the calculated value of 0.38–0.41 $Å^{-1}$ from Ref. 27.

While the BB has $Q=2k_F$ nesting, its distribution is nearly the same as that for the band of the freestanding In bilayer. This fact and the charge-density distribution of the BB shown in Fig. 5 reveal that the BB has p character and is strongly localized around the In atoms. The BB does not cause Peierls transition because it exists inside the bulk band continuum and its amplitude around the surface is lower at the crossing point with Fermi energy.

B. Pb/Cu(001)

In the Pb/Cu(001) system, a fully reversible phase transition from the split c(2×2) structure that can be seen for coverage of 0.5–0.6 ML to a $c(5\sqrt{2}\times\sqrt{2})R45°$ structure was observed at 440 K, and the well-nested Fermi surface of the split c(2×2) structure partially disappeared for the low-temperature phase below 440 K.[25] The $c(5\sqrt{2}\times\sqrt{2})R45°$ structure is produced by insertion of antiphase boundaries into the rigid c(2×2) structure and having all Pb atoms located at hollow sites of the Cu(001) substrate.[48] Although the CDW transition occurs for coverage of 0.5–0.6 ML, we re-

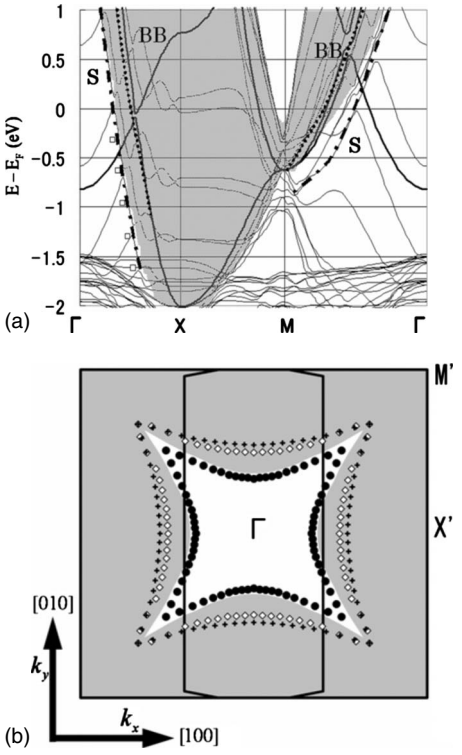

FIG. 6. (a) Band structure of Pb/Cu(001)-c(2×2). The broad lines represent the band structure of the freestanding Pb layer. The dotted-dashed and dotted lines are the surface resonance states S and the states induced by the Pb atom, respectively. The band structure of a surface resonance state measured by PES (Ref. 25) is shown by small squares. (b) Fermi surface of the surface states on the Pb/Cu(001)-0.5 ML structure. The large square and small polygon represent the surface Brillouin-zone boundaries of the c(2×2) and c($5\sqrt{2}\times\sqrt{2}$)*R*45° structures, respectively. The filled circles, open diamonds, and crosses show the positions of S1, BB, and the bands of the freestanding Pb layer crossing the Fermi energy. The shaded area represents the projected bulk band of clean Cu(001).

strict our study to Pb/Cu(001)-0.5 ML because the low-energy electron-diffraction pattern of the split c(2×2) structure is similar to that of the rigid c(2×2) structure and shows that Pb atoms are located at the hollow sites.[25] Our calculation result for a rigid c(2×2) phase shows that Pb atoms located at the hollow sites of the Cu(001) surface are stable, which is consistent with the results of previous works.[28,45] The height of the Pb monolayer above the Cu surface layer agrees reasonably well with the experimental value,[25] as shown in Table I.

Figure 6(a) shows the calculated band structure of the c(2×2) phase for Pb/Cu(001)-0.5 ML. We see that the BB is in the bulk band continuum and it relates to the *p* orbital of Pb. These characteristics of the BB are similar to those in the case of In/Cu(001)-0.5 ML. The energy of the bulk band edge (i.e., S) is less than that of the clean Cu(001) surface. The energy distribution of S agrees well with the plots from PES for the surface resonance state of Pb/Cu(001)-0.6 ML.[25] Although the charge-density distribution of band S is similar to that of the bulk band B at Γ point, the distribution gradually changes to that of the surface state near the crossing point with the Fermi energy. Figure 6(b) shows the Fermi surfaces of S, BB, and the band of the freestanding Pb layer. The wave number of the nesting vector of the Fermi surface relating to band S is 0.29 Å^{-1}, and this value is in good agreement with the experimental value of 0.29 Å^{-1}.[25] As a result, S can be assigned as the surface resonance state observed by PES. From the above two features of S (i.e., the nesting vector determined from the surface resonance states and the large charge density at the Fermi energy), we conclude that the Peierls transition from c(2×2) to c($5\sqrt{2}\times\sqrt{2}$)*R*45° is caused by the S band in the Pb/Cu(001)-0.5 ML system. This means that there is a common fundamental mechanism for the transitions of In and Pb on Cu(001).

The calculated Fermi wave number (0.288 Å^{-1}) differs from the boundary of the Brillouin zone (0.346 Å^{-1}) for the low-temperature phase. Joco *et al.*[25] reported that the energy level of the center of the surface band gap is below the Fermi level, and its wave number corresponds to the boundary of the c($5\sqrt{2}\times\sqrt{2}$)*R*45° Brillouin zone. Therefore the Fermi wave number of the state S should be smaller than the boundary value of the Brillouin zone. When the electron-phonon coupling is strong, the center of the surface band gap is not equivalent to the Fermi energy.[13] Therefore one can expect sufficient strength of electron-phonon interactions.

The calculated Fermi surface of the BB is similar to that of the freestanding Pb layer, and it is revealed that the wave function relating to the BB is localized around the Cu-Pb interatomic region. Note that the wave number of the nesting vector, 0.427 Å^{-1}, is very different from the experimental value and the BB lies in the bulk band continuum. Hence, the BB is not the band that is observed by PES and causes the CDW transition.

C. Bi/Cu(001)-0.5 ML

Cu(001) covered with 0.5 ML Bi also has a phase transition from the c(2×2) phase to the c($9\sqrt{2}\times\sqrt{2}$)*R*45° phase.[29] While there is no clear evidence for the formation of a band gap by the well-nested surface state, the c($9\sqrt{2}\times\sqrt{2}$)*R*45° phase has a domain-wall structure of the c(2×2) phase as does Pb/Cu(001)-0.5 ML.[46] As a result, it is suggested that Bi/Cu(001)-0.5 ML undergoes CDW transition.[12] However, the phase transition of this system depends on the coverage rather than the temperature[29] and it is considered as a first-order phase transition.[49] In the present study, we applied the calculation procedure we used for In/Cu(001) and Pb/Cu(001) to Bi/Cu(001) and compared the CDW transition mechanism of Bi/Cu(001) with that of In/Cu(001) and that of Pb/Cu(001). The hollow site is stable for Bi absorption just as for In and Pb, and the results are summarized in Table I.

Figure 7(a) shows the band structure of the c(2×2) phase of Bi/Cu(001)-0.5 ML. The features of the band structure are basically the same as those of Pb/Cu(001)-0.5 ML, but the energies of S and the band of the freestanding Bi layer are much lower than those of Pb/Cu(001)-0.5 ML, especially along the Γ−M′ line. This affects the shape of the Fermi surface of S as shown in Fig. 7(b); it is nearly square and similar to the Fermi surface of the freestanding Bi layer. The Fermi wave number is 0.27 Å^{-1}, which is not commensurate

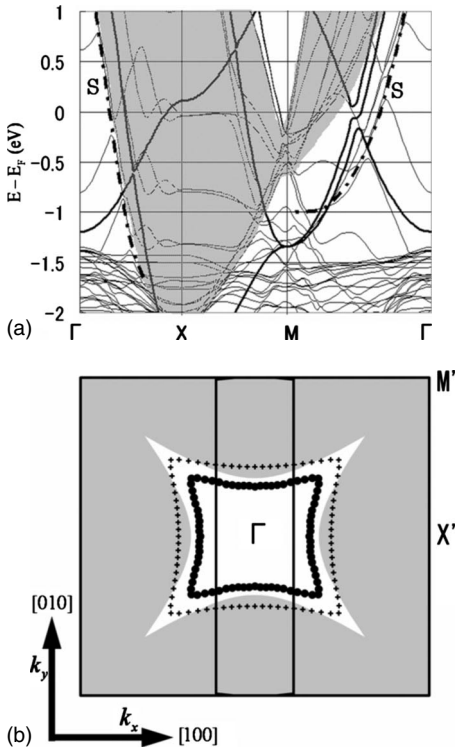

FIG. 7. (a) Band structure of Bi/Cu(001)-0.5 ML. The broad lines represent the band structure of the freestanding Bi layer. The dotted-dashed lines are the surface resonance states S. (b) Fermi surface of the surface states on the Bi/Cu(001)-0.5 ML structure. The large square and small polygon show the surface Brillouin-zone boundaries of the $c(2\times2)$ and $c(9\sqrt{2}\times\sqrt{2})R45°$ structures, respectively. The filled circles and crosses show the positions of S1 and the bands of the freestanding Pb layer crossing the Fermi energy. The shaded area represents the projected bulk band of clean Cu(001) as shown in Fig. 5.

with the boundary of the Brillouin zone of the $c(9\sqrt{2}\times\sqrt{2})R45°$ phase at 0.19 $Å^{-1}$. This similarity between the two Fermi surfaces suggests that the electron states of free Bi atoms gain energy through the interaction with the electron states of the Cu(001) surface but they keep the properties of the freestanding Bi layer. That is, in the Bi/Cu(001)-0.5 ML system, the interactions between Bi atoms dominate those between Bi atoms and the Cu substrate. The charge-density distribution of S at Γ point is highly localized around Bi atoms [see Fig. 3(c)] and has the character of the surface state. Moreover, band S maintains the character of the surface state throughout the Brillouin zone, which is in contrast to the behavior of S1 for In/Cu(001) or S for Pb/Cu(001), which changes to surface states only around the Fermi energy.

The surface state S seems to be the result of "direct coupling" between the free Bi and the Cu bulk band B rather than the change in potential because of the adsorption of adatoms. Since the surface state produced by In or Pb is triggered by the change in potential, the present surface state has a different nature. However, we found that S produces a well-nested Fermi surface and is not commensurate with the Brillouin zone of the low-symmetry phase; thus, there is the possibility that the CDW transition can be rationalized by the strong electron-phonon coupling.

The present calculations at least predict that the origin of the surface state of Bi/Cu(001)-0.5 ML is different from that of In or Pb/Cu(001). The mechanism of the transition of the former differs from that of the latter where the Cu(001) surface leads the transition.

IV. COMPARISON OF VIBRONIC COUPLINGS FOR In/Cu(001) AND W(001)

As stated in Sec. III, the *sp*-hybrid band constructed by the adsorbed metal atoms and substrate (bulk) Cu plays a role in the CDW transitions in In/Cu(001) and Pb/Cu(001). These two systems are classified as Peierls transitions having strong (electron-phonon) coupling while they should be distinguished from a typical case such as that of W(001) because of the spatial coherence length as described in Sec. II. However, it is difficult to estimate the coherence length quantitatively and clarify its contribution to the Peierls transition by means of first-principles calculations. Hence, we adopt the real-space view throughout the analysis, although real-space and *k*-space approaches are basically equivalent. Furthermore, in the real-space approach, there is the possibility of identifying the "promoting mode (coordinate)" in the CDW transition. In the real-space view, the Peierls transition can be described by the JTE.[50–52] Since formation of the band gap and related lattice distortion can be directly linked by the JTE, we apply the JTE scheme to vibronic couplings of short-coherence and long-coherence systems, which relate to W(001) and In/Cu(001), respectively, and then discuss the difference in terms of the JTE.

First, we focus on W(001) as the prototype of strong coupling and short coherence (see Sec. II). Our frozen-phonon calculations are summarized as follows. The optimized structure of the $p(1\times1)$ unit cell has a negative mode at M point of the Brillouin zone. When we simply construct the $c(2\times2)$ cell by collocating the above optimized $p(1\times1)$ cell as the minimum cell, a negative mode appears at Γ point in the normal mode analysis of the $c(2\times2)$ system. This means that the high-symmetry $c(2\times2)$ phase, which consists of the ordered $p(1\times1)$ cell as described above, is *not* stable. If we relax the above constraint [i.e., the full geometric optimization is applied to the $c(2\times2)$ structure], W atoms of the top layer are laterally displaced and zigzag chains proposed by Debe and King form.[53] The deviation from the high symmetry is 0.24 Å along the surface plane (0.24 ± 0.0025 Å from experiment[54]) and less than 0.01 Å along the surface vertical. We checked the normal modes and found that there is no negative mode throughout the Brillouin zone for the fully optimized $c(2\times2)$ structure. These results are in good agreement with previous results.[15,18] All calculations for W(001) surfaces were performed using SIESTA software and the conditions were the same as those stated for In/Cu(001)-0.5 ML in Sec. II.

We found four negative modes at Γ point in the $c(2\times2)$ structure, which we denote **Q**1, **Q**2, **Q**3, and **Q**4, where set **Q**1 is degenerate with **Q**2 and set **Q**3 is degenerate with **Q**4. The frequencies have the order $\mathbf{Q}1=\mathbf{Q}2<\mathbf{Q}3=\mathbf{Q}4$. The *z*

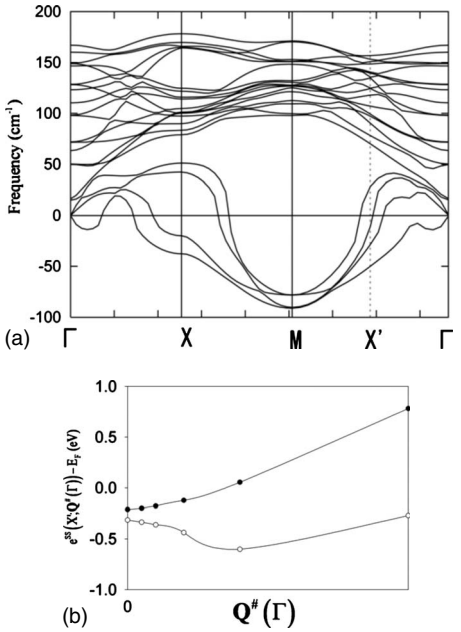

FIG. 8. (a) Phonon dispersion curves of the W(001)-p(1×1) structure. X′ is the midpoint of the Γ−M line. There are four negative modes at point M. (b) Plots of $e^{SS}[X';\mathbf{Q}^{\#}(\Gamma)]$ calculated for the W(001)-c(2×2) structure. $e^{SS}[X';\mathbf{Q}^{\#}(\Gamma)]$ is the energy of the surface-state band at X′ point as a function of the normal-mode vector $\mathbf{Q}^{\#}(\Gamma)$. $\mathbf{Q}^{\#}(\Gamma)=0$ is the high-symmetry structure. The lines are only for the purpose of clarity.

axis is set in the direction perpendicular to the surface and the *x* axis and *y* axis are taken parallel to the surface. By exchanging the *x* axis and *y* axis, $\mathbf{Q}1(\mathbf{Q}2)$ is mapped to $\mathbf{Q}2(\mathbf{Q}1)$, and $\mathbf{Q}3(\mathbf{Q}4)$ is mapped to $\mathbf{Q}4(\mathbf{Q}3)$. The only difference between $(\mathbf{Q}1,\mathbf{Q}2)$ and $(\mathbf{Q}3,\mathbf{Q}4)$ is the relative phase between two slab sides. Hence, as long as we focus on one side of the slab (and this is physically natural), the four modes are equivalent. Since the present model of In/Cu(001)-0.5 ML is one-sided adsorption on the slab, we consider the normal mode on one side and compare the results for W(001) with those for In/Cu(001)-0.5 ML. Let us take the displacements only on one side of the slab to represent negative modes at Γ point, which we denote $\mathbf{Q}^{\#}(\Gamma)$. W atoms on the top layer shift in the [010] direction by $\mathbf{Q}^{\#}(\Gamma)$. The dispersion curve of the surface state of W(001)-p(1×1) structure crosses the Fermi level around the midpoint of Γ−M or X′, which is the new Brillouin-zone boundary relating to the c(2×2) structure. Hence, we calculated the band energy of the surface states at point X′ as a function of the normal-mode coordinate of $\mathbf{Q}^{\#}(\Gamma)$, which is denoted $e^{SS}[X';\mathbf{Q}^{\#}(\Gamma)]$ [SS refers to the surface states of W(001)], and found that the degenerate surface states split into two bands as shown in Fig. 8(b). While the upper band has upward dispersion, the lower band has a minimum and then rises along $\mathbf{Q}^{\#}(\Gamma)$, which corresponds to going from higher to lower symmetry (symmetry breaking). The plots of $e^{SS}[X';\mathbf{Q}^{\#}(\Gamma)]$ show that the symmetry breaking by real-space displacements of surface atoms of W(001) resolves the degeneracy of the surface-state band, which is related to the structure of the surface. Since the split of bands occurs around the Fermi energy and the upper band becomes unoccupied along $\mathbf{Q}^{\#}(\Gamma)$, the lowering of energy of the lower band contributes to a decrease in total energy. These behaviors are in good agreement with the picture of the JTE for the solid-state problem. Since $Q^{\#}(\Gamma)$ is valid only around the equilibrium high-symmetry structure, the maximum band gap of 1.15 eV in Fig. 8(b) is smaller than that of the completely relaxed c(2×2) structure, 1.8 eV. Nevertheless, Fig. 8(b) clearly shows that $\mathbf{Q}^{\#}(\Gamma)$ induces initial stabilization with the breaking of symmetry. In other words, we can identify the mode $\mathbf{Q}^{\#}(\Gamma)$ as the "promoting mode" of the CDW transition in W(001) on the basis of the Jahn-Teller picture.

We applied the same normal-mode analysis to In/Cu(001)-0.5 ML to analyze the CDW transition mechanism but we could not find negative modes throughout the Brillouin zone of the c(2×2) cell. However, a recent model calculation showed that phonons of small wave vectors decomposing the nesting vector are involved in the higher-order process.[55] Therefore, the above simple mode analysis restricted to the unit c(2×2) cell is insufficient, and we can expect the large $(9\sqrt{2}\times 2\sqrt{2})R45°$ cell to be unstable because of collective modes of its periodicity. However, our calculation result shows that the $(9\sqrt{2}\times 2\sqrt{2})R45°$ structure produced by the collocation of high-symmetry c(2×2) cells was stable. There is no distortion of the lattice or movement of In atoms from their equilibrium positions. In other words, none of the surface-localized phonon modes of the $(9\sqrt{2}\times 2\sqrt{2})R45°$ structure decrease the total energy of the system; thus, we find no clear evidence of the instability.

Nevertheless, as the next step, we focus on the electron-phonon coupling between the surface state and a few distinct modes in the surface Brillouin zone of the $(9\sqrt{2}\times 2\sqrt{2})R45°$ structure found as candidates for the promoting modes. Some acoustic-phonon bands are slightly softened at the surface Brillouin-zone edge X″ (see Fig. 1). This suggests that one or more of these modes may contribute to the phase transition of In/Cu(001), and, hence, we apply the analysis of vibronic coupling as described above. Since there are real and imaginary solutions for the normal-mode vector at points other than Γ, we define the real displacement vector as

$$\mathbf{Q}^{R}(\mathbf{q}) = \frac{1}{2}[\mathbf{Q}(\mathbf{q}) + \mathbf{Q}(-\mathbf{q})],$$

$$\mathbf{Q}^{I}(\mathbf{q}) = \frac{i}{2}[\mathbf{Q}(\mathbf{q}) - \mathbf{Q}(-\mathbf{q})], \tag{3}$$

where $\mathbf{Q}[\mathbf{q}(\neq 0)]$ denotes the normal-mode vector for wave number $\mathbf{q}$. $\mathbf{Q}(\mathbf{q})$ has complex components. We adopt the value of X″ as the wave number because we find a few distinct modes on it. In addition, we take one of the normal-mode vectors of the softened modes as a candidate of the promoting mode since the direction of this vector is expected to be mostly related to the CDW ground state (see the scanning tunneling microscopy image in Ref. 20). We denote these vectors $\mathbf{Q}^{R}(X'')$ and $\mathbf{Q}^{I}(X'')$ and show them in Figs. 9(c) and 9(d). $\mathbf{Q}^{R}(X'')$ and $\mathbf{Q}^{I}(X'')$ contain the displacement relating to the transfers between the hollow sites and In at-

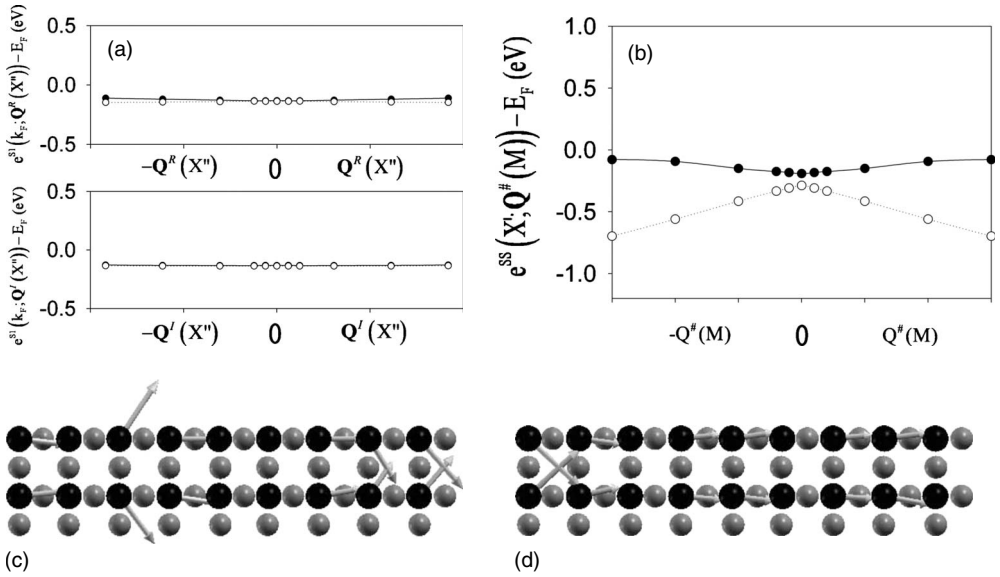

FIG. 9. (a) Plots of $e^{S1}[k_F;\mathbf{Q}^R(\mathrm{X}'')]$ (upper graph) and $e^{S1}[k_F;\mathbf{Q}^I(\mathrm{X}'')]$ (bottom graph), which are the energy of S1 at k_F as functions of the normal-mode vectors $\mathbf{Q}^R(\mathrm{X}'')$ and $\mathbf{Q}^I(\mathrm{X}'')$, respectively. Two bands degenerated for the high-symmetry $[\mathbf{Q}^{R,I}(\mathrm{X}'')=0]$ structures are displayed by open and filled circles. (b) Plots of $e^{SS}[\mathrm{X}';\mathbf{Q}^{\#}(\mathrm{M})]$ along $\mathbf{Q}^{\#}(\mathrm{M})$ for the W(001)-p(1×1) structure. [(c) and (d)] Normal-mode vectors $\mathbf{Q}^R(\mathrm{X}'')$ and $\mathbf{Q}^I(\mathrm{X}'')$, respectively. Cu atoms are shown by gray spheres and only for the first layer for clarity. The black spheres are In atoms.

oms interacting with each other in the surface plane.

For comparison, we also analyzed vibronic coupling between the surface state and promoting modes for W(001)-p(1×1) at M point, where we find largely negative modes. While there are four negative modes at M point as shown in Fig. 8(a), they are actually equivalent as discussed in the analysis of Γ point. Since $\mathbf{Q}^R(\mathrm{M})$ and $\mathbf{Q}^I(\mathrm{M})$ are equivalent in the present case, we followed the same procedure as for Γ point; i.e., we took only the displacement on one side of the slab from $\mathbf{Q}^R(\mathrm{M})$, which has the lowest frequency. We refer to this vector as $\mathbf{Q}^{\#}(\mathrm{M})$. Clearly, one can regard $\mathbf{Q}^{\#}(\mathrm{M})$ as the promoting mode because of its negative frequency. The direction of vectors of $\mathbf{Q}^{\#}(\mathrm{M})$ is slightly deviated from that of $\mathbf{Q}^{\#}(\Gamma)$.

We calculated the band energies of surface states of both In/Cu(001) and W(001) at k points, where the formations of the band gaps will be found along their candidates of promoting modes. These k points are k_F for In/Cu(001) and X′ for W(001). One can find k_F around $1/3\Gamma-\mathrm{X}'$, which is the boundary of the $(9\sqrt{2}\times 2\sqrt{2})R45°$ Brillouin zone shown in Fig. 4. Next, we plotted $e^{S1}[k_F;\mathbf{Q}^R(\mathrm{X}'')]$, $e^{S1}[k_F;\mathbf{Q}^I(\mathrm{X}'')]$, and $e^{SS}[\mathrm{X}';\mathbf{Q}^{\#}(\mathrm{M})]$ as the functions of the relating normal-mode vector as shown in Figs. 9(a) and 9(b). While these modes belong to a point that is not Γ, we neglected the phase relationship between the unit cell and supercell when we calculated phonon dispersion. To express displacements along $\mathbf{Q}^{\#}(\mathrm{M})$, we prepared the p(2×2) cell of W(001) because $\mathbf{Q}^{\#}(\mathrm{M})$ is a mode of M point. The W atom belonging to one of the p(1×1) units of the whole system is then displaced. For In/Cu(001), we calculated $e^{S1}[k_F;\mathbf{Q}^R(\mathrm{X}'')]$ and $e^{S1}[k_F;\mathbf{Q}^I(\mathrm{X}'')]$ within the $(9\sqrt{2}\times 2\sqrt{2})R45°$ cell on the basis of the frozen-phonon approximation.

The energy plots for In/Cu(001)-0.5 ML and W(001) differ dramatically. In the case of W(001), $\mathbf{Q}^{\#}(\mathrm{M})$, which causes the breaking of symmetry, resolves the degeneracy of the surface states. Although $\mathbf{Q}^{\#}(\mathrm{M})$ cannot represent $\mathbf{Q}^{\#}(\Gamma)$, which relates directly to the promoting mode of the CDW transition, $e^{SS}[\mathrm{X}';\mathbf{Q}^{\#}(\mathrm{M})]$ splits by as much as about 0.6 eV. There is clear evidence of the JTE even if the displacement vector is slightly shifted from the vector of the mode at Γ point for W(001).

On the other hand, for In/Cu(001)-0.5 ML, collective modes do not affect the band dispersion. Nevertheless, the $(9\sqrt{2}\times 2\sqrt{2})R45°$ structure is sufficiently large to express the change of surface state caused by the pairing of In atoms. Although we checked other surface-localized modes, band dispersions are little changed by lattice distortions, as shown in Fig. 9(a). In our calculations, the maximum "gap" between the surface states of In/Cu(001)-0.5 ML (recall that this gap is not the band gap) is less than 0.04 eV, which is only about 6.7% of the gap between the surface states in W(001). The energy value of 0.04 eV is close to the limit of the numerical accuracy in our calculation; hence, we conclude that the static JTE is negligible for In/Cu(001)-0.5 ML. In other words, static displacements of the lattice do not induce obvious instability for the $(9\sqrt{2}\times 2\sqrt{2})R45°$ structure of In/Cu(001)-0.5 ML, although the CDW transition is observed by experiment. Neither static displacements nor structural optimizations from various initial guesses produced stable structures. As a result, one can consider that the Born-Huang term and/or high-order nonadiabatic correction terms, which consist of the derivative of the electronic wave function by lattice (ion) coordinates, are required to find the practical potential-energy minimum of the ground state in the present system.[56,57] In this case, the phase transition of In/Cu(001)-0.5 ML should be triggered by the dynamic JTE, where the electron-ion coupled (vibronic) state is created through the nonadiabatic (derivative) coupling term. This dy-

namic effect resolves the degeneracy of the electronic bands and reduces the total energy further.

The static JTE caused by short-range interactions in real space triggers a CDW and produces the incommensurate periodicity of the CDW, large band gap, order-disorder character and the "soft" band-gap edge. Here, the terminology soft means that the k space, where the band gap is generated, becomes broad. In the case of In/Cu(001)-0.5 ML, the first three characteristics are observed, but the band-gap edge is sharp as for a weak-coupling CDW. Therefore, the dynamic JTE is expected to be related to the coherence length of the CDW. Our calculation suggests that the vibronic coupling is strong for W(001) and weak for In/Cu(001) in the sense of static interaction, although a "large band gap" is observed for In/Cu(001)-0.5 ML (at least 400 meV). Thus, it is possible that the coherence length of the CDW correlates to the strength of the static JTE.

Here, we discuss our results and those obtained at the same level of theory [DFT with Born-Oppenheimer (BO) approximation] by Johannes and Mazin.[6] They suggested that the **k**-dependent electron-phonon coupling is dominant in the case of the one-dimensional chain of Na atoms. This system is characterized by a zigzag ground state with no band gap. In such a case, the description using only the **k**-dependent electron-phonon coupling should be valid. In the case of In/Cu(001), while the formation of the band gap was experimentally observed, neither the gap formation nor the energy stabilization was found with static JTE. Therefore we conclude that the nonadiabatic (dynamical) coupling would be relevant for In/Cu(001), at variance with the case of the Na 1D chain.

V. CONCLUSION

We conclude that In/Cu(001)-0.5 ML and Pb/Cu(001)-0.5 ML have the same mechanism of CDW transition from the fact that they have the same origin for the well-nested Fermi surface. If an In or Pb atom adsorbs on a Cu(001) surface, the change in the potential near the surface decreases the energy of the bulk band composing the edge of the projected bulk bands. This band has the character of a surface state because it enters the projected bulk band gap through a decrease in energy. While it has a distribution similar to that of the bulk band, it has large amplitude of wave functions around the surface in the narrow range around the Fermi energy. Moreover, the calculated Fermi wave vectors agree well with those determined from experiments. These band features show that the surface states are identical to those observed in PES. The Fermi surfaces of the surface states have quasisquare shapes and distributions similar to those of the edge of the bulk band gap. This shows that the surface state is split from the bulk band and has its origin in the Cu(001) surface. Consequently, it is the surface resonance state resulting from both bulk and adsorbates that causes the CDW transition and modifies the $c(2\times2)$ phase. Thus, we support the experimental prediction that an adsorbate layer on the Cu(001) surface triggers CDW transition with theoretical calculation. In addition, we conclude that the surface resonance state suggested in Ref. 27 has a character of adsorbate atoms and is not identical to that observed in PES.

Bi has an electron structure similar to that of In or Pb, but Bi/Cu(001)-0.5 ML does not have a Fermi surface with a distribution similar to that of the edge of the bulk band gap, while all systems occur the phase transitions from $c(2\times2)$. Considering these results, we can state that although a Cu(001) surface is prone to CDW transition triggered by an adsorbate layer, the adsorbate needs to employ the same mechanism as for In/Cu(001) or Pb/Cu(001). That is, the interaction between adsorbates needs to be weaker than that between adsorbate and substrate. The quantitative evaluation of these conditions can be achieved by the calculation of the overlap integral around the surface but this is a future task.

A comparison of the vibrational coupling of In/Cu(001)-0.5 ML with that of W(001) revealed an obvious difference. W(001), which is a case of a strong-coupling and short-coherence CDW, has promoting modes $Q^{\#}(\Gamma)$ and $Q^{\#}(M)$ for its high-symmetry $c(2\times2)$ and $p(1\times1)$ structures, respectively. The energies of surface-state bands of W(001) as functions of promoting modes show the JTE; i.e., the bands split around the Fermi energy according to the breaking of symmetry. A low-symmetry $c(2\times2)$ structure is energetically stable and its energy increases if atoms move toward the high-symmetry structure. On the other hand, in the case of a strong-coupling and long-coherence CDW, such as that of In/Cu(001)-0.5 ML, we could not find an obvious instability for the $(9\sqrt{2}\times2\sqrt{2})R45°$ structure. Furthermore, while we found candidates of promoting modes at points that were not Γ in the Brillouin zone, these modes did not affect the surface-state band structure. These behaviors of surface states suggest that the static JTE for In/Cu(001) is negligible. However, there must be a mechanism of stabilization of the CDW ground state that is found to be stable at low temperature by experiments.[12,13,20,21] Therefore, we conclude that the dynamic JTE, where the nonadiabatic coupling becomes crucial, contributes to the phase transition of In/Cu(001)-0.5 ML. Since the most distinctive difference in the CDW between In/Cu(001) and W(001) is the broadness of the k region where the band gap forms (i.e., the correlation length), the coherence length of the CDW should relate to the dynamic nature of the JTE. Moreover, the origin of the "strong-coupling" nature of In/Cu(001) comes under question because our calculation did not support there being a strong electron-phonon interaction of In/Cu(001) like there is for W(001). We expect that the dynamic nature will contribute to the "large band gap" of In/Cu(001) observed by experiment. The determination of a clearer relationship among the dynamic nature of the JTE, the correlation length, and the strength of electron-phonon coupling is the focus of future work.

ACKNOWLEDGMENTS

Authors thank G. Giorgi for fruitful discussions. This research was supported by a Grant-in-aid for Scientific Research on Priority Area No. 2003801 (H.N.) from MEXT of Japan and by Grant-in-aid for Scientific Research (C) No. 20613002 (H.N.) and (A) No. 21245004 (K.Y.) from JSPS.

*ooto@tcl.t.u-tokyo.ac.jp
†Corresponding author; hs-nakamura@aist.go.jp

[1] S. Kagoshima, H. Nagasawa, and T. Takahashi, *Teijigen-Doutai (Low-Dimensional Conductors)* (Shokabo, Tokyo, 2000).
[2] G. Grunner, *Density Waves on Solids* (Addison-Wesley, Reading, MA, 1994).
[3] J. M. Carpinelli, H. H. Weitering, E. W. Plummer, and R. Stumpf, Nature (London) **381**, 398 (1996).
[4] J. M. Carpinelli, H. H. Weitering, M. Bartkowiak, R. Stumpf, and E. W. Plummer, Phys. Rev. Lett. **79**, 2859 (1997).
[5] S. Hatta, H. Okuyama, M. Nishijima, and T. Aruga, Appl. Surf. Sci. **237**, 270 (2004).
[6] M. D. Johannes and I. I. Mazin, Phys. Rev. B **77**, 165135 (2008).
[7] M. D. Johannes, I. I. Mazin, and C. A. Howells, Phys. Rev. B **73**, 205102 (2006).
[8] M. Calandra, I. I. Mazin, and F. Mauri, Phys. Rev. B **80**, 241108(R) (2009).
[9] J. Avila, Y. Huttel, A. Mascaraque, G. Le Lay, E. G. Michel, and M. C. Asensio, Surf. Sci. **435**, 327 (1999).
[10] J. Avila, A. Mascaraque, E. G. Michel, and M. C. Asensio, J. Electron Spectrosc. Relat. Phenom. **103**, 361 (1999).
[11] J. Avila, A. Mascaraque, E. G. Michel, M. C. Asensio, G. LeLay, J. Ortega, R. Perez, and F. Flores, Phys. Rev. Lett. **82**, 442 (1999).
[12] T. Aruga, J. Phys.: Condens. Matter **14**, 8393 (2002).
[13] T. Aruga, Surf. Sci. Rep. **61**, 283 (2006).
[14] T. Aruga and S. Hatta, Butsuri (in Japanese), **63**, 178 (2008).
[15] X. W. Wang and W. Weber, Phys. Rev. Lett. **58**, 1452 (1987).
[16] H. J. Ernst, E. Hulpke, and J. P. Toennies, Phys. Rev. Lett. **58**, 1941 (1987).
[17] H. J. Ernst, E. Hulpke, and J. P. Toennies, Phys. Rev. B **46**, 16081 (1992).
[18] R. Yu, H. Krakauer, and D. Singh, Phys. Rev. B **45**, 8671 (1992).
[19] W. K. Han, S. C. Ying, and D. Sahu, Phys. Rev. B **41**, 4403 (1990).
[20] T. Nakagawa, G. I. Boishin, H. Fujioka, H. W. Yeom, I. Matsuda, N. Takagi, M. Nishijima, and T. Aruga, Phys. Rev. Lett. **86**, 854 (2001).
[21] T. Nakagawa, S. Mitsushima, H. Okuyama, M. Nishijima, and T. Aruga, Phys. Rev. B **66**, 085402 (2002).
[22] S. Hatta, H. Okuyama, M. Nishijima, and T. Aruga, Phys. Rev. B **71**, 041401(R) (2005).
[23] S. Hatta, H. Okuyama, T. Aruga, and O. Sakata, Phys. Rev. B **72**, 081406(R) (2005).
[24] T. Nakagawa, H. Okuyama, M. Nishijima, T. Aruga, H. W. Yeom, E. Rotenberg, B. Krenzer, and S. D. Kevan, Phys. Rev. B **67**, 241401(R) (2003).
[25] V. Joco, J. Martinez-Blanco, P. Segovia, T. Balasubramanian, J. Fujii, and E. G. Michel, Surf. Sci. **600**, 3851 (2006).
[26] J. Martínez-Blanco, V. Joco, H. Ascolani, A. Tejeda, C. Quirós, G. Panaccione, T. Balasubramanian, P. Segovia, and E. G. Michel, Phys. Rev. B **72**, 041401(R) (2005).
[27] X. Gao, Y. Zhou, S. Wu, and D. Wang, Phys. Rev. B **66**, 073405 (2002).
[28] A. Sánchez and S. Ferrer, Phys. Rev. B **39**, 5778 (1989).
[29] F. Delamare and G. E. Rhead, Surf. Sci. **35**, 172 (1973).
[30] W. Kohn and L. J. Sham, Phys. Rev. **140**, A1133 (1965).
[31] D. Vanderbilt, Phys. Rev. B **41**, 7892 (1990).
[32] G. Kresse and J. Joubert, Phys. Rev. B **54**, 11169 (1996).
[33] P. E. Blöchl, Phys. Rev. B **50**, 17953 (1994).
[34] G. Kresse and J. Joubert, Phys. Rev. B **59**, 1758 (1999).
[35] J. Perdew, J. Chevary, S. Vosko, K. Jackson, M. Pederson, D. Singh, and C. Fiolhais, Phys. Rev. B **46**, 6671 (1992).
[36] H. Monkhorst and J. Pack, Phys. Rev. B **13**, 5188 (1976).
[37] C. Kittel, *Introduction to Solid State Physics* (Maruzen, Tokyo, 2001).
[38] O. Jepsen, D. Glotzel, and A. R. Mackintosh, Phys. Rev. B **23**, 2684 (1981).
[39] A. Euceda, D. M. Bylander, L. Kleinman, and K. Mednick, Phys. Rev. B **27**, 659 (1983).
[40] J. M. Soler, E. Artacho, J. D. Gale, A. Garcia, J. Junquera, P. Ordejon, and D. Sanchez-Portal, J. Phys.: Condens. Matter **14**, 2745 (2002).
[41] J. P. Perdew, K. Burke, and M. Ernzerhof, Phys. Rev. Lett. **78**, 1396 (1997).
[42] N. Troullier and J. L. Martins, Phys. Rev. B **43**, 8861 (1991).
[43] L. Kleinman and D. M. Bylander, Phys. Rev. Lett. **48**, 1425 (1982).
[44] M. Jiang, Y. J. Zhao, and P. L. Cao, Phys. Rev. B **57**, 10054 (1998).
[45] W. Hosler, W. Moritz, E. Tamura, and R. Feder, Surf. Sci. **171**, 55 (1986).
[46] H. L. Meyerheim, M. D. Santis, W. Moritz, and I. K. Robinson, Surf. Sci. **418**, 295 (1998).
[47] K. Momma and F. Izumi, J. Appl. Crystallogr. **41**, 653 (2008).
[48] W. Li, J.-S. Lin, M. Karimi, and G. Vidali, J. Vac. Sci. Technol. A. **9**, 1707 (1991).
[49] P. Wynblatt, D. Chatain, and A. Ranguis, Surf. Sci. **601**, 1623 (2007).
[50] Y. D. Chuang, A. D. Gromko, D. S. Dessau, T. Kimura, and Y. Tokura, Science **292**, 1509 (2001).
[51] R. Hoffman, *Solids and Surfaces: A Chemist's View of Bonding in Extended Structures* (VCH, New York, 1989).
[52] I. B. Bersuker, *The Jahn-Teller Effect* (Cambridge University Press, UK, 2006).
[53] M. K. Debe and D. A. King, Phys. Rev. Lett. **39**, 708 (1977).
[54] M. S. Altman, P. J. Estrup, and I. K. Robinson, Phys. Rev. B **38**, 5211 (1988).
[55] T. Hamano and Y. Ono, Physica E **22**, 156 (2004).
[56] M. Born and K. Huang, *Dynamical Theory of Crystal Lattice* (Oxford University Press, Oxford, 1954).
[57] Y. E. Perlin and M. Wagner, *The Dynamical Jahn-Teller Effect in Localized Systems* (North-Holland, Amsterdam, 1984).